Investigation of the leakage mechanism in solar-blind AlGaN p-i-n photodetector at high reverse bias

Zhaolan Sun,[1,2] ID Jing Yang,[1,a)] ID Degang Zhao,[1,3,a)] ID Zongshun Liu,[1] ID Lihong Duan,[1] Feng Liang,[1] ID Ping Chen,[1] Bing Liu,[4,a)] ID Fu Zheng,[4] and Xuefeng Liu[4] ID

AFFILIATIONS

[1]Laboratory of Solid State Optoelectronic Information Technology, Chinese Academy of Sciences, Institute of Semiconductors, Beijing 100083, China
[2]College of Materials Science and Opto-Electronic Technology, University of Chinese Academy of Sciences, Beijing 100049, China
[3]School of Electronic, Electrical and Communication Engineering, University of Chinese Academy of Sciences, Beijing 100049, China
[4]Key Laboratory of Electronics and Information Technology for Space Systems, National Space Science Center, Chinese Academy of Sciences, Beijing 100190, China

[a)]Authors to whom correspondence should be addressed: yangjing333@semi.ac.cn, dgzhao@red.semi.ac.cn, and lbing@nssc.ac.cn

ABSTRACT

The leakage mechanism of solar-blind AlGaN p-i-n photodetectors has been investigated. By studying the temperature-dependent I–V curves, we determined that Poole–Frenkel emission is the main source of the leakage current, and the corresponding trap energy level is 0.61 eV. Cathodoluminescence measurement demonstrates that the leakage current of the device may be related to the deep-level traps in the p-AlGaN layer. An analysis of deep-level transient spectroscopy testing results for p-AlGaN suggests that nitrogen vacancies formed during the epitaxial growth of high Al-content p-AlGaN act as electron traps. The trap potential energy decreases at high reverse bias voltage, making trapped electrons easier to escape, which increases the leakage current.

I. INTRODUCTION

Recently, the solar-blind AlGaN photodetectors have attracted extensive research interest due to their applications in biochemical warning, corona monitoring, biomedical imaging, ultraviolet astronomy, and so on.[1–3] Among them, p-i-n AlGaN photodetectors have been widely studied because of their advantages of low working bias, rapid response, low leakage current, and strong integration capability.[4] However, high Al-content AlGaN films have been proven to be difficult to grow by MOCVD systems due to large lattice mismatch to foreign substrates, low surface mobility of Al atoms, and difficulty of doping due to AlGaN having a wider bandgap.[2,5] Point defects can affect AlGaN-based device performance as sources of non-recombination centers. In 2020, Rathkanthiwar *et al.* showed that the V-pits originating in the

AlN nucleation layer are associated with leakage paths in GaN HEMTs, and the mechanism for vertical leakage is speculated to be occurring through the higher oxygen concentration.[6] In 2021, Reddy *et al.* demonstrated two types of point-defect traps as the primary source of reverse leakage before breakdown in Al-rich AlGaN.[7] The high leakage current that occurs at high reverse bias will significantly deteriorate device performance, and it is necessary to examine the source to provide a control path for the development of solar-blind AlGaN-based photodetectors.

In this study, we have investigated the point defects of solar-blind AlGaN p-i-n photodetector using high-resolution x-ray diffraction (HRXRD) measurement, temperature-dependent current-voltage (I–V) curves, cathodoluminescence (CL), and deep-level transient spectroscopy (DLTS). The results have shown that the nitrogen

vacancies formed during p-AlGaN layer growth dominate the leakage current in solar-blind AlGaN p-i-n photodetector. It will help to understand the characteristics of point defects in high Al-content AlGaN films and the significance of further controlling point defects for improving the performance of devices.

II. EXPERIMENT

The back-illuminated solar-blind p-i-n AlGaN photodetector T0 was grown on a double-polished 2 in. sapphire substrate through metal-organic chemical vapor deposition (MOCVD). In sample T0, an AlN buffer layer was deposited on the c-plane sapphire substrate first, followed by an AlN template, then a $1\,\mu m$ thick heavily Si-doped n-$Al_{0.65}Ga_{0.35}N$ layer, a 100 nm thick undoped i-$Al_{0.5}Ga_{0.5}N$ layer, and a 300 nm thick Mg-doped p-$Al_{0.5}Ga_{0.5}N$ layer. The schematic diagram of the device structure for sample T0 is shown in Fig. 1. After the material growth, the p-type dopants were activated by rapid thermal annealing at 900 °C for 3 min in N_2 ambient. The mesa structure was then formed by inductively coupled plasma etching. A SiO_2 layer as the passivation layer is deposited to suppress sidewall leakage. A 10/10 nm Ni/Au semitransparent electrode contact film was deposited on the p-AlGaN layer, which was annealed at 550 °C for 5 min to form an ohmic contact. Finally, Ti/Al/Ti/Au (15/150/50/250 nm) layers were deposited on both Ni/Au semitransparent film and n-AlGaN layer to form p-type and n-type electrodes. Finally, the sample T0 was cut with an area of $45 \times 45\,\mu m^2$ by a splitting process. The full width at half maximum (FWHM) at (002) and (102) reflection was obtained by ω-scan rocking curves of HRXRD. The temperature-dependent I–V tests were performed using a Keithley 2400 source meter under dark conditions, and the temperature was controlled from 200 to 350 K on a probe station. The CL
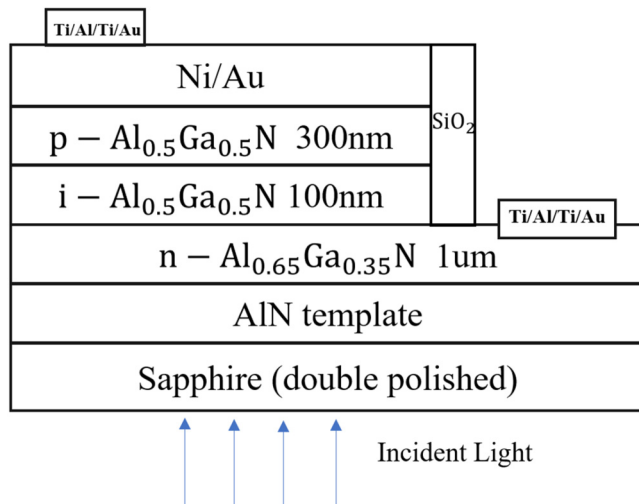
spectra were measured at room temperature with different electron accelerating voltages. The DLTS were carried out in the temperature range of 80–500 K using a DLTS system.

III. RESULTS AND DISCUSSION

By a Gaussian fitting curve to the ω-scan rocking curves, we can obtain that the full width at half maxima (FWHM) of the XRD (002) and (102) reflections are 309 and 581 arcsec for the n-AlGaN layer and 440 and 612 arcsec for the p/i-AlGaN layer. The observed increase in the FWHM at the 002 reflection can be attributed to the increased dislocation density, which may lead to local lattice distortion, an increase in point defects, and other irregularities in the lattice structure.

Next, we performed the I–V tests at room temperature under light and dark conditions. The I–V curves are shown in Fig. 2(a). During the measurement of light I–V curve of the device, the incident light ($\lambda = 260$ nm) illuminated the bottom side of the sapphire substrate. It is indicated that the dark current (black) and light current (red) curves were nearly indistinguishable and showed a strong dependence on voltage after the reverse bias voltage exceeds −20 V. The reverse leakage current appearing at higher voltage is significant, and there is a necessity to determine its source and find the pathway to control it for the development of solar-blind AlGaN-based photodetectors. To study the carrier transport mechanism of the solar-blind AlGaN p-i-n photodetector, the I–V curves measured over a temperature range of 200–350 K in dark conditions were tested and depicted in Fig. 2(b). The I–V curves measured at varying temperature tables have a larger noise level and were able to be measured only at higher temperatures. It is noted that this leakage current was field-dependent and temperature-dependent. It increases at higher reverse bias voltage and at high temperatures.

The combination of electric field and temperature dependencies of the I–V curves indicates an effect like Poole–Frenkel emission (PFE), in which the Coulomb potential energy of the carrier in a trapping center can be reduced by an applied electric field across the dielectric film and by an increase in temperature. The reduction in potential energy may increase the probability of a carrier being thermally excited out of the trap into the conduction band of the semiconductor.[8,9] That can explain why the PF emission is strongly dependent on the electric field and temperature, and the current related to PFE is given by[7,10]

$$J \propto E \exp\left(\frac{-q\phi}{kT}\right) \times \exp\left(\frac{q}{kT}\left(\frac{q}{\pi\varepsilon}\right)^{0.5} E^{0.5}\right). \quad (1)$$

In the high reverse bias voltage, the width of the depletion region can be considered a constant, hence

$$\ln\left(\frac{I}{U}\right) \propto -\frac{q\phi}{kT} + \left(\frac{q}{kT}\left(\frac{q}{\pi\varepsilon}\right)^{0.5} U^{0.5}\right), \quad (2)$$

where J represents the current density, E represents the electric field in the semiconductor depletion region, ϕ represents the trap energy level (the barrier height for carrier emission from the trap state), q is the electron charge, k is the Boltzmann factor, T is the temperature, ε is the dielectric constant, I represents the current, and U represents

FIG. 1. The schematic diagram of the back-illuminated solar-blind p-i-n AlGaN photodetector T0.

The figure labels read: Ti/Al/Ti/Au; Ni/Au; p − $Al_{0.5}Ga_{0.5}N$ 300nm; SiO_2; i − $Al_{0.5}Ga_{0.5}N$ 100nm; Ti/Al/Ti/Au; n − $Al_{0.65}Ga_{0.35}N$ 1um; AlN template; Sapphire (double polished); Incident Light
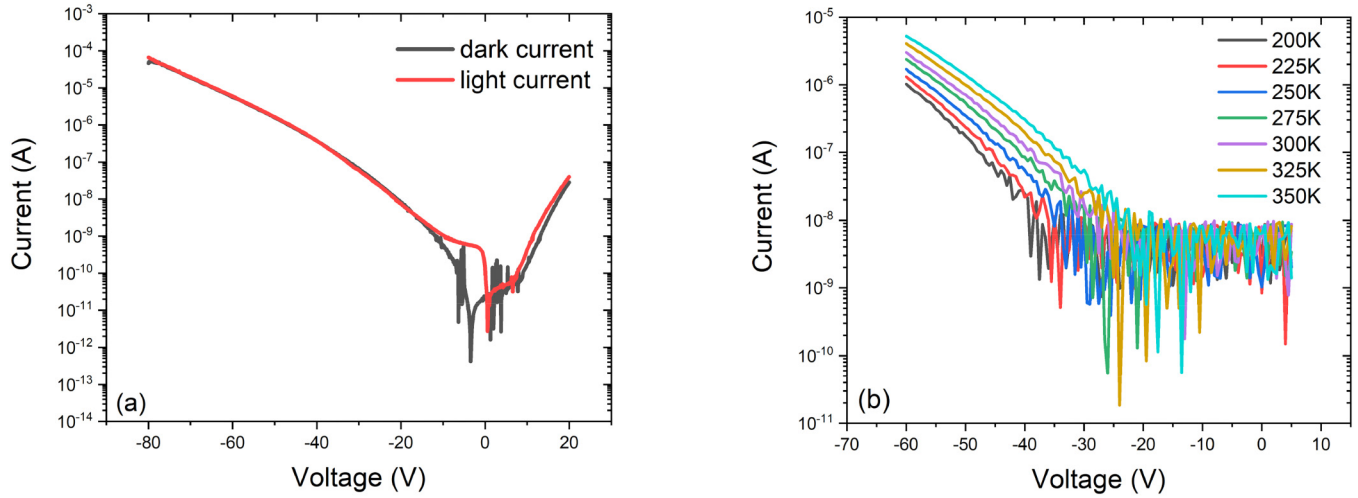
FIG. 2. (a) I–V curves of a 45×45 μm^2 AlGaN p-i-n photodetector in the dark and under 260 nm illumination at room temperature. (b) Temperature-dependent I–V curves of the 45×45 μm^2 AlGaN p-i-n photodetector in dark conditions.

the voltage. Hence, if the leakage current is due to the Poole–Frenkel emission of carriers excited from the electron traps, $\ln\left(\frac{I}{U}\right)$ should be a linear function of $U^{0.5}$. Figure 3(a) exhibits $\ln\left(\frac{I}{U}\right)$ as a function of $U^{0.5}$ for the I–V curves over the temperature range of 200–350 K, and the inset shows the $\ln\left(\frac{I}{U}\right)$ vs $U^{0.5}$ curves at room temperature. The inset in Fig. 3(a) is measured at room temperature to mitigate the noise introduced by the temperature-dependent test system, and the leakage current at low bias voltage is measurable. All of them follow a linear change, which confirms that PFE is the dominant mechanism for the leakage current of the device.

Furthermore, to investigate the traps, we employ Eq. (2). The y-intercept for the plot of $\ln\left(\frac{I}{U}\right)$ vs $U^{0.5}$ curve is given by

$$\text{y-intercept} = a - \phi\left(\frac{q}{kT}\right), \tag{3}$$

where a is a constant. Therefore, plotting the y-intercept as a function of q/kT can reveal the trap energy level in its slope. As shown in Fig. 3(b), a deep state was found at 0.61 eV in device T0. At high bias voltage, the Coulomb barrier at the center of the trap
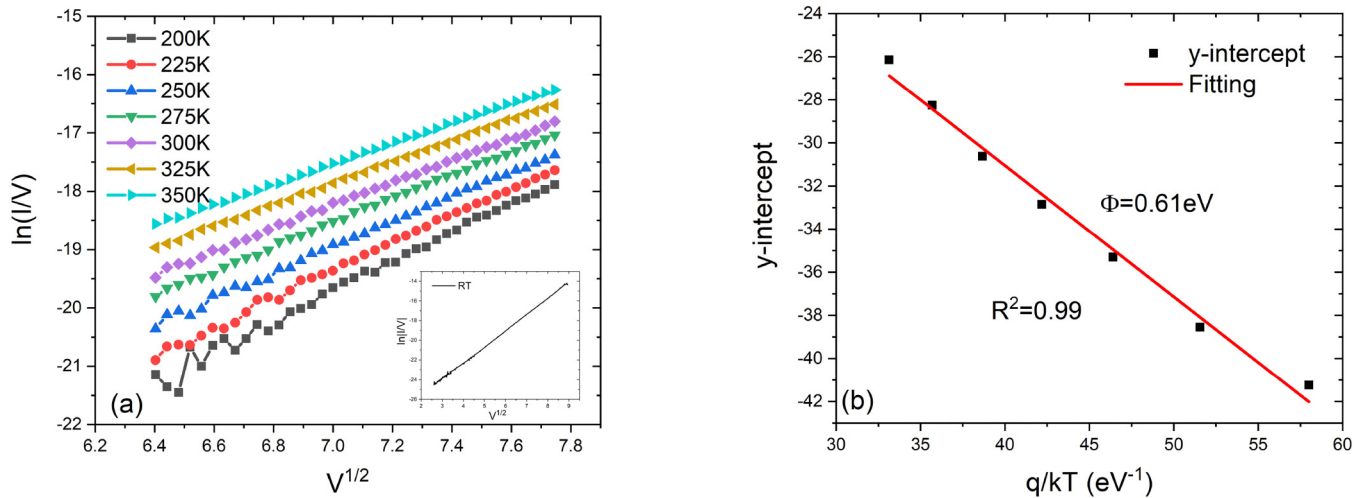

FIG. 3. (a) Derived $\ln\left(\frac{I}{U}\right)$ vs $U^{0.5}$ curves employing PFE as carrier transport mechanism at high bias voltages for device T0. The inset is the $\ln\left(\frac{I}{U}\right)$ vs $U^{0.5}$ curve at room temperature. (b) Linear fit of parameter y-intercept vs q/kT for device T0.

decreases, which leads to an increase in the carrier emission rate in the center of the trap, making it easier for the trapped carriers to be excited to the conduction band or valance band, and ultimately resulting in an increase in leakage current. Some research groups suggest that the trapped energy close to 0.61 eV may originate from point defects such as oxygen impurities, Fe contaminations, carbon-related impurities, Mg-related impurities, or nitrogen vacancies.[11–14] Because the deep-level traps have a great influence on the current leakage, they should be mainly located in the depletion region, in the i-AlGaN layer, or in the p-AlGaN layer with a wide depletion region due to the low doping efficiency of high Al-content AlGaN.[15]

Since the penetration depth of the electron beam during the CL measurement increases with increasing electron accelerating energy, to examine the impurity luminescence peak at different penetration depths,[16] we have measured the CL spectra using different electron accelerating voltages. In this case, the structural and optical properties of different layers in the multilayer structure can be identified.[17] Figure 4(a) shows the CL spectra of the sample T0 with different energies of the incident electrons, where the accelerating voltage is at 5, 10, and 12 kV, respectively. The penetration depth is correspondingly p-AlGaN layer, upper i-AlGaN layer, and lower i-AlGaN layer, respectively. In Fig. 4(a), the 4.4 eV peak corresponds to the band edge emission of the p-AlGaN layer or the i-AlGaN layer, which intensity is used as the normalized peak intensity. Then, the impurity peak intensities at 3.76 and 2.66 eV are compared to check the distribution location of corresponding impurity levels. With the operation voltage of 5 kV, the majority of the collected CL signals are from the p-AlGaN layer, which displays an impurity peak of 3.76 eV. Based on

the doping concentrations of n-AlGaN, i-AlGaN, and p-AlGaN being 5×10^{18}, 1×10^{16}, and 5×10^{16} cm^{-3}, respectively, the energy band diagram and electric field distribution diagram of the device T0 at 0 V are obtained, as shown in Fig. 4(b). It can be seen that the high electric field is mainly distributed in the p-AlGaN layer and i-AlGaN layer. These two layers are in the depletion region, which dominates the leakage current. At high reverse bias voltage, the trapped carriers are excited to the conduction band, resulting in an increase in leakage. It is shown that the impurity of 3.76 eV in p-Al$_{0.5}$Ga$_{0.5}$N may originate from Mg-related impurities or nitrogen vacancies.[18] With increasing operation voltage to 10 and 12 kV, an additional impurity peak of 2.66 eV appears, which should come from the i-AlGaN layer. Some research groups have shown that it may originate from carbon impurity or Al/Ga vacancy, whose emission peak may be caused by the transition of donor–acceptor (DA) pair recombination.[19–23] In fact, the impurity energy level related to the 3.76 eV peak is located at 0.64 eV, which value is close to 0.61 eV. According to the trap energy level (0.61 eV) derived by the PFE mechanism, we conclude that the leakage current of device T0 is related to the deep-level traps from the p-AlGaN layer.

The capacitance transient deep-level transient spectroscopy DLTS method, which has been extensively discussed and utilized for characterizing deep-level defects,[24,25] was used to characterize electrically active defects in the p-AlGaN layer. The device was operated at a forward bias of 2 V. Since the metal and p-AlGaN have formed a Schottky junction, a depletion region is created in the p-AlGaN layer under forward bias. A fill pulse of 0 V is used to populate traps in the depletion region. The activation energy (E_a) and capture cross section (σ_n) of defect states that appeared in DLTS spectra were obtained by the Arrhenius plot following the equation[26,27]
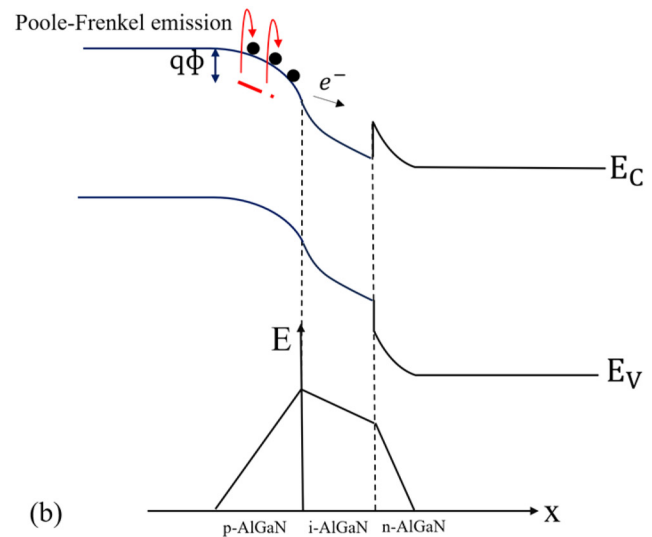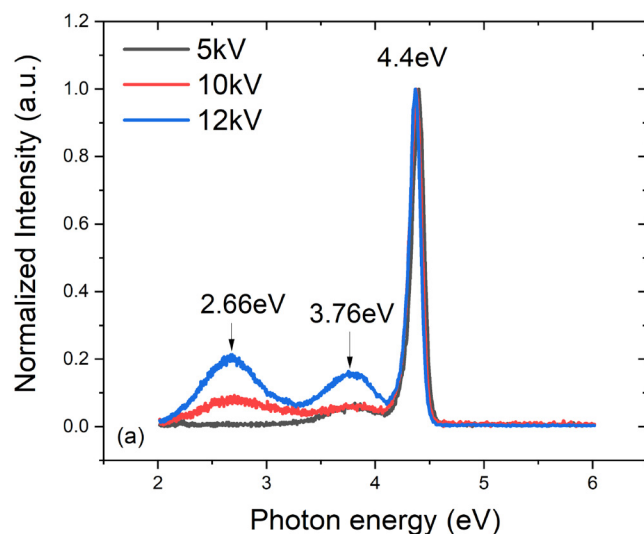
FIG. 4. (a) The CL spectra of device T0 at different electron accelerating voltages of 5 kV (black), 10 kV (red), and 12 kV (blue). (b) Schematic energy band diagram of Poole–Frenkel emission and electric field diagram in device T0 at high reverse bias condition.
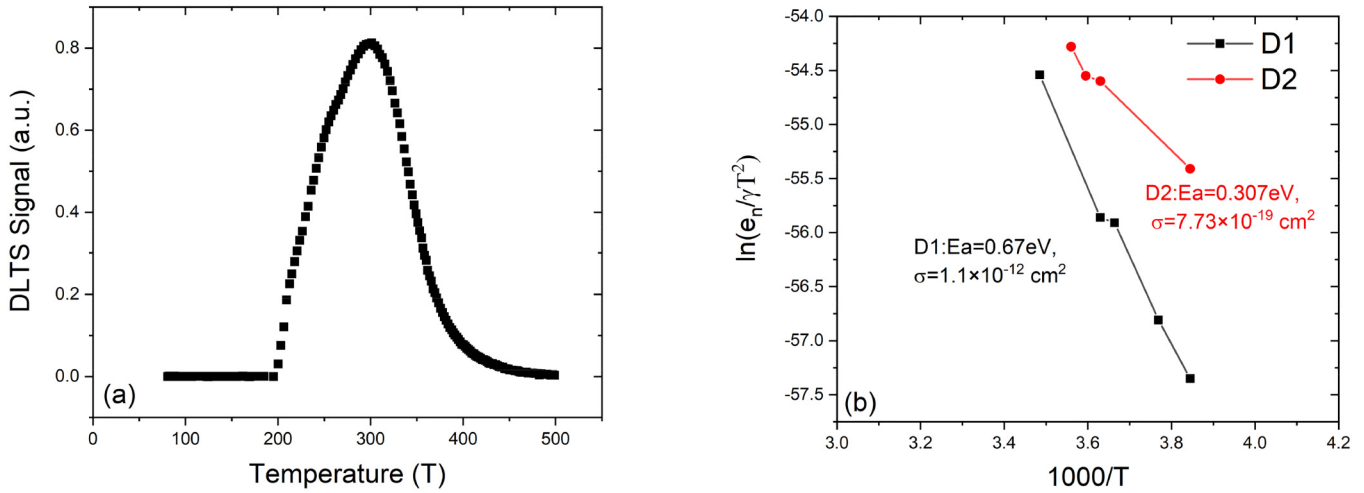
02 November 2024 07:03:55

FIG. 5. (a) DLTS signal at a forward bias of 2 V of the device T0. (b) Arrhenius plot of the device T0 for two deep-level activation energies D1 (black square) and D2 (red circle). The lines connecting the dots are used for eye view.

$$\ln\left(\frac{e_n}{\gamma T^2}\right) = -\frac{E_a}{kT} + \ln(\sigma_n). \qquad (4)$$

Here, $\gamma = \frac{4\sqrt{6}k^2\pi^{3/2}m_n^*}{h^3}$, is a constant, e_n is the emission rate, and T is the measured temperature. The capture cross section (σ_n) directly reflects the capture efficiency of free carriers in the trap center. Figure 5(a) shows a raw DLTS signal over a temperature range of 80–500 K. For DLTS, a positive peak is related to minority-carriers trap levels, whereas a negative peak is related to majority-carriers trap levels.[28,29] For the p-AlGaN layer of the device T0, the positive peak indicates an electron trap. As shown in Fig. 5(b), the parameters of two deep levels D1 and D2 were obtained by using Eq. (4). The activation energy E_a values of D1 and D2 are 0.67 and 0.307 eV above the valance band, respectively. The cross section σ_n values of D1 and D2 are 1.1×10^{-12}, and 7.73×10^{-19} cm^2, respectively. It indicates that the electrons emitted by the D1 trap are significantly more than the D2 trap at high bias voltage, and the former has a more important impact on device leakage. It is also noticed that the trap energy level obtained by DLTS spectra and PFE mechanism examination is very consistent, indicating that the D1 trap dominates the leakage current of device T0. Relevant studies have shown that high Al-content p-type AlGaN films are inclined to generate nitrogen vacancies due to lower formation energy in the epitaxial growth process, and the impurity peak in p-Al$_{0.5}$Ga$_{0.5}$N films is about 3.6 eV.[13,18] Therefore, we can conclude that the nitrogen vacancies and related complexes, which act as electron traps in the high Al-content p-AlGaN layer, are the main source of T0 leakage at high bias voltage.

The results indicate the need for suppressing the nitrogen vacancies to improve device performance. It is found that nitrogen vacancies have small formation energy in GaN-based materials, and its concentration decreases with increasing V/III ratio.[14,30,31] In addition, the decrease in nitrogen vacancy density may also enhance the conductivity of p-AlGaN film. This finding is important for reducing the concentration of nitrogen vacancies and improving device performance.

IV. CONCLUSION

In conclusion, we have investigated the leakage mechanism of solar-blind AlGaN p-i-n photodetector. By studying the dark current I–V curves, we have identified that Poole–Frenkel emission of carriers activated from the electron traps is the main source of the leakage current. Further research shows that the nitrogen vacancies formed in high Al-content p-AlGaN during epitaxial growth act as electron traps, and the trap potential energy decreases at a high reverse bias voltage, which leads to the trapped electrons being more easily emitted, and thus the leakage current increases. This study shows that point defects play an important role in the leakage current of solar-blind AlGaN photodetectors, which may have great significance in controlling the point defects related to the performances of the devices.

AUTHOR DECLARATIONS

Conflict of Interest

The authors have no conflicts to disclose.

Author Contributions

Zhaolan Sun: Conceptualization (equal); Formal analysis (equal); Writing – original draft (lead); Writing – review & editing (equal). **Jing Yang:** Conceptualization (equal); Supervision (equal); Writing – review & editing (equal). **Degang Zhao:** Conceptualization (equal); Formal analysis (equal); Supervision (equal); Writing – review & editing (equal). **Zongshun Liu:** Resources (equal). **Lihong Duan:** Resources (equal). **Feng Liang:** Writing – review & editing (equal). **Ping Chen:** Writing – review & editing (equal). **Bing Liu:** Funding acquisition (equal). **Fu Zheng:** Funding acquisition (equal). **Xuefeng Liu:** Funding acquisition (equal).

DATA AVAILABILITY

The data that support the findings of this study are available within the article.

REFERENCES

[1]P. Kung, A. Yasan, R. McClintock, S. Darvish, K. Mi, and M. Razeghi, "Future of Al$_x$Ga$_{1-x}$N materials and device technology for ultraviolet photodetectors," Proc. SPIE **4650** (2002).

[2]R. Tan, Q. Cai, J. Wang, D. Pan, Z. Li, and D. Chen, "Highly solar-blind ultraviolet selective metal-semiconductor-metal photodetector based on back-illuminated AlGaN heterostructure with integrated photonic crystal filter," Appl. Phys. Lett. **118**(14), 142105 (2021).

[3]W. Li, Y. Wang, G. Gu, F. Ren, D. Zhou, W. Xu, D. Chen, R. Zhang, Y. Zheng, and H. Lu, "Polarization-assisted AlGaN heterostructure-based solar-blind ultraviolet MSM photodetectors with enhanced performance," IEEE Trans. Electron Devices **70**(7), 3468–3474 (2023).

[4]Y. Gu, Q. Fan, Y. Liu, X. Yang, X. Jiang, J. Guo, X. Zhang, N. Lu, G. Chen, and G. Yang, "High-temperature forward and reverse current transport mechanisms of AlGaN-based solar-blind UV photodetector," IEEE Trans. Electron Devices **69**(12), 6804–6810 (2022).

[5]S. Zhu, J. Yan, Y. Zhang, J. Zeng, Z. Si, P. Dong, J. Li, and J. Wang, "The effect of delta-doping on Si-doped Al rich n-AlGaN on AlN template grown by MOCVD," Phys. Status Solidi C **11**(3–4), 466–468 (2014).

[6]S. Rathkanthiwar, A. Kalra, N. Remesh, A. Bardhan, R. Muralidharan, D. N. Nath, and S. Raghavan, "Impact of pits formed in the AlN nucleation layer on buffer leakage in GaN/AlGaN high electron mobility transistor structures on Si (111)," J. Appl. Phys. **127**(21), 215705 (2020).

[7]P. Reddy, D. Khachariya, W. Mecouch, M. H. Breckenridge, P. Bagheri, Y. Guan, J. H. Kim, S. Pavlidis, R. Kirste, S. Mita, E. Kohn, R. Collazo, and Z. Sitar, "Study on avalanche breakdown and Poole–Frenkel emission in Al-rich AlGaN grown on single crystal AlN," Appl. Phys. Lett. **119**(18), 182104 (2021).

[8]R. B. Hall, "The Poole-Frenkel effect," Thin Solid Films **8**(4), 263–271 (1971).

[9]F.-C. Chiu, "A review on conduction mechanisms in dielectric films," Adv. Mater. Sci. Eng. **2014**, 1–18 (2014).

[10]Z. Dai, Y. Liu, G. Yang, F. Xie, C. Zhu, Y. Gu, N. Lu, Q. Fan, Y. Ding, Y. Li, Y. Yu, and X. Zhang, "Carrier transport and photoconductive gain mechanisms of AlGaN MSM photodetectors with high Al content," Chin. Opt. Lett. **19**(8), 082504 (2021).

[11]A. Y. Polyakov, N. B. Smirnov, A. V. Govorkov, A. V. Markov, A. M. Dabiran, A. M. Wowchak, A. V. Osinsky, B. Cui, P. P. Chow, and S. J. Pearton, "Deep traps responsible for hysteresis in capacitance-voltage characteristics of AlGaN/GaN heterostructure transistors," Appl. Phys. Lett. **91**(23), 232116 (2007).

[12]M. Cho, Z. Xu, M. Bakhtiary-Noodeh, H. Jeong, C.-W. Tsou, T. Detchprohm, R. D. Dupuis, and S.-C. Shen, "Effective leakage current reduction in GaN ultraviolet avalanche photodiodes with an ion-implantation isolation method," IEEE Trans. Electron Devices **68**(6), 2759–2763 (2021).

[13]J. L. Lyons, D. Wickramaratne, and C. G. Van De Walle, "A first-principles understanding of point defects and impurities in GaN," J. Appl. Phys. **129**(11), 111101 (2021).

[14]D. Johnstone, "Summary of deep level defect characteristics in GaN and AlGaN," Proc. SPIE **6473** (2007).

[15]Q. Cai, W. K. Luo, Q. Li, M. Li, D. J. Chen, H. Lu, R. Zhang, and Y. D. Zheng, "Algan ultraviolet avalanche photodiodes based on a triple-mesa structure," Appl. Phys. Lett. **113**(12), 123503 (2018).

[16]J. I. Goldstein, D. E. Newbury, and J. R. Michael, *Scanning Electron Microscopy and X-Ray Microanalysis* (Springer, 2017).

[17]Z. Ma, A. Almalki, X. Yang, X. Wu, X. Xi, J. Li, S. Lin, X. Li, S. Alotaibi, and L. Zhao, "The influence of point defects on AlGaN-based deep ultraviolet LEDs," J. Alloys Compd. **845**, 156177 (2020).

[18]J. Hyun Kim, P. Bagheri, R. Kirste, P. Reddy, R. Collazo, and Z. Sitar, "Tracking of point defects in the full compositional range of AlGaN via photoluminescence spectroscopy," Phys. Status Solidi A **220**(8), 2200390 (2023).

[19]T. A. Henry, A. Armstrong, A. A. Allerman, and M. H. Crawford, "The influence of Al composition on point defect incorporation in AlGaN," Appl. Phys. Lett. **100**(4), 043509 (2012).

[20]N. Liu, Q. Wang, B. Li, J. Wang, K. Zhang, C. He, L. Wang, L. Song, X. Cao, B. Wang, D. Lin, X. Liu, W. Zhao, Z. Gong, and Z. Chen, "Point-defect distribution and transformation near the surfaces of AlGaN films grown by MOCVD," J. Phys. Chem. C **123**(14), 8865–8870 (2019).

[21]F. Liang, D. Zhao, D. Jiang, Z. Liu, J. Zhu, P. Chen, J. Yang, S. Liu, Y. Xing, L. Zhang, and M. Li, "Carbon-related defects as a source for the enhancement of Yellow luminescence of unintentionally doped GaN," Nanomaterials **8**(9), 744 (2018).

[22]F. Liang, D. Zhao, D. Jiang, Z. Liu, J. Zhu, P. Chen, J. Yang, S. Liu, Y. Xing, and L. Zhang, "Role of Si and C impurities in yellow and blue luminescence of unintentionally and Si-doped GaN," Nanomaterials **8**(12), 1026 (2018).

[23]R. Y. Korotkov, M. A. Reshchikov, and B. W. Wessels, "Acceptors in undoped GaN studied by transient photoluminescence," Physica B **325**, 1–7 (2003).

[24]M. J. Legodi, S. S. Hullavarad, S. A. Goodman, M. Hayes, and F. D. Auret, "Defect characterization by DLTS of AlGaN UV Schottky photodetectors," Physica B **308–310**, 1189–1192 (2001).

[25]S. DasGupta, O. Slobodyan, T. Smith, A. Binder, J. Flicker, R. Kaplar, J. Mueller, L. Garcia Rodriguez, and S. Atcitty, "Identification of the defect dominating high temperature reverse leakage current in vertical GaN power diodes through deep level transient spectroscopy," Appl. Phys. Lett. **120**(5), 053502 (2022).

[26]M. Lee, C. W. Ahn, T. K. O. Vu, H. U. Lee, E. K. Kim, and S. Park, "First observation of electronic trap levels in freestanding GaN crystals extracted from Si substrates by hydride vapour phase epitaxy," Sci. Rep. **9**(1), 7128 (2019).

[27]C. W. Ahn, S. Park, and E. K. Kim, "Effect of oxygen on defect states of Al$_{0.4}$Ga$_{0.6}$N layers grown by hydride vapor phase epitaxy," J. Mater. Res. Technol. **17**, 1485–1490 (2022).

[28]D. V. Lang, "Deep-level transient spectroscopy: A new method to characterize traps in semiconductors," J. Appl. Phys. **45**(7), 3023–3032 (1974).

[29]D. Monti, M. Meneghini, C. De Santi, G. Meneghesso, E. Zanoni, J. Glaab, J. Rass, S. Einfeldt, F. Mehnke, J. Enslin, T. Wernicke, and M. Kneissl, "Defect-related degradation of AlGaN-based UV-B LEDs," IEEE Trans. Electron Devices **64**(1), 200–205 (2017).

[30]M. L. Nakarmi, N. Nepal, C. Ugolini, T. M. Altahtamouni, J. Y. Lin, and H. X. Jiang, "Correlation between optical and electrical properties of Mg-doped AlN epilayers," Appl. Phys. Lett. **89**(15), 152120 (2006).

[31]F. Li, J. Liu, A. Tian, X. Li, X. Zhang, and H. Yang, "Nitrogen vacancies in GaN templates and their critical role on the luminescence efficiency of blue quantum wells," Opt. Express **31**(9), 14937 (2023).

02 November 2024 07:03:55